



PAPER

OPEN ACCESS

RECEIVED
30 December 2025REVISED
16 February 2026ACCEPTED FOR PUBLICATION
17 March 2026PUBLISHED
31 March 2026

Original content from this work may be used under the terms of the [Creative Commons Attribution 4.0 licence](#).

Any further distribution of this work must maintain attribution to the author(s) and the title of the work, journal citation and DOI.



A discrete-time benchmark for assessing critical slowing down indicators

Sajad Jafari^{1,2}, Anitha Karthikeyan³, Mahtab Mehrabbeik¹ , Karthikeyan Rajagopal^{4,5} , Veli Baysal⁶ and Matjaž Perc^{7,8,9,10,*}

¹ Department of Biomedical Engineering, Amirkabir University of Technology (Tehran Polytechnic), Tehran, Iran

² Health Technology Research Institute, Amirkabir University of Technology (Tehran Polytechnic), Tehran, Iran

³ Center for Cognitive Science, Trichy SRM Medical College Hospital and Research Center, Trichy, India

⁴ Center for Research, Easwari Engineering College, Chennai, India

⁵ Center for Research, SRM TRP Engineering College, Trichy, India

⁶ Department of Computer Engineering, Bartın University, 74100 Bartın, Türkiye

⁷ Faculty of Natural Sciences and Mathematics, University of Maribor, Koroška Cesta 160, 2000 Maribor, Slovenia

⁸ Community Healthcare Center Dr Adolf Drolc Maribor, Ulica Talcev 9, 2000 Maribor, Slovenia

⁹ Department of Physics, Kyung Hee University, 26 Kyungheedaero, Dongdaemun-gu, Seoul 02447, Republic of Korea

¹⁰ University College, Korea University, 145 Anam-ro, Seongbuk-gu, Seoul 02841, Republic of Korea

* Author to whom any correspondence should be addressed.

E-mail: matjaz.perc@gmail.com

Keywords: early warning signal, critical slowing down indicators, hysteresis, chaos

Abstract

We introduce a low-dimensional, discrete-time benchmark for evaluating critical slowing down indicators and early-warning signals in the presence of complex dynamics. Starting from a map-based attention-deficit-disorder model, we add a bias offset to obtain a modified system with a controllable, hysteresis-like coexistence band. Within this band, forward and backward parameter sweeps follow distinct branches, and abrupt switching can occur alongside periodic windows and chaotic regimes. We characterize the dynamics using state-space portraits, bifurcation diagrams, and Lyapunov exponents. We then evaluate four metric-based indicators—lag-1 autocorrelation, variance, skewness, and kurtosis—using a period-aware computation designed for regimes beyond period-one. We find that variance exhibits the most consistent warning trend near the coexistence boundaries, whereas autocorrelation is more susceptible to spurious spikes. Higher-order moments are generally less reliable, particularly in intermittently chaotic regions. Overall, the benchmark is computationally efficient and provides a practical testbed for stress-testing early-warning methods and for quantifying sensitivity to analysis choices.

1. Introduction

Critical slowing down (CSD) refers to the progressive loss of resilience that many dynamical systems exhibit as they approach a critical transition (tipping point), typically associated with a local bifurcation where a stable state becomes weakly attracting [1, 2]. As recovery from small perturbations becomes slower, the system's dominant return rate decreases, leading to characteristic statistical footprints in observed time series that can serve as early warning signals (EWS) [3, 4]. Common CSD-based indicators include increasing lag-1 autocorrelation (reflecting longer memory), rising variance (reflecting amplified fluctuations), longer relaxation times, and, in some settings, changes in skewness, kurtosis, or spectral reddening due to the shift of power toward low frequencies [5, 6]. In practice, EWS are usually estimated within moving windows and interpreted as trends rather than absolute values; however, their reliability depends strongly on noise structure, sampling rate, window length, nonstationarity, and confounding mechanisms that can generate similar patterns without an impending bifurcation. Consequently, rigorous validation and comparison of EWS methods require controlled benchmark systems with known stability structure and tunable proximity to criticality.

Different studies have examined CSD indicators on real-world datasets and compared their performance under practical constraints. For example, Mehrabbeik *et al* [7] evaluated lag-1 autocorrelation, variance, skewness, and kurtosis as candidate CSD indicators using electroretinogram recordings from salamander eyes, with contrast and flash frequency acting as bifurcation parameters. Their results identified variance as the most promising indicator, yielding the highest true-positive rate with the fewest false positives; they further reported that lag-1 autocorrelation achieved comparable true-positive performance but suffered from elevated false-positive rates, thereby reducing its overall reliability. In a related context, Lenton *et al* [8] compared two widely used CSD-based early warning approaches, including lag-1 autocorrelation and detrended fluctuation analysis (DFA), by re-analyzing six established test beds: three palaeoclimate time series approaching abrupt deglacial transitions and three model-based experiments in which the Atlantic thermohaline circulation is gradually forced into collapse. Importantly, they showed that early-warning performance can be sensitive to common analysis choices, including aggregation, detrending, window length, and filtering, which may strengthen or weaken the apparent slowing-down signature across different records. They emphasized that autocorrelation-based and DFA-based diagnostics have complementary strengths and limitations, and recommended combining multiple indicators (including variance when relevant) to increase robustness and reduce dependence on any single analysis setting. In a different application domain, Diks *et al* [9] evaluated three commonly used early-warning indicators, including lag-1 autocorrelation, lag-1 mutual information (MI) as a nonlinear dependence measure, and standard deviation (variance proxy), on financial time series preceding several major crises. Overall, they found that early-warning performance was inconsistent across events: some datasets exhibited upward trends consistent with CSD, but many did not, and results depended on the series and preprocessing. They also highlighted that apparent warnings can be spurious, particularly for MI-based measures that do not account for changes in the marginal distribution, underscoring the need for careful statistical controls when applying CSD indicators to real-world financial data. Similar examples have been reported across diverse application domains, including depression [10–13] and broader mental health symptoms [14], sandstone failure [15], collapse in mutualistic communities [16], abrupt environmental change [17–19], seizure susceptibility [20, 21], and physical systems [22].

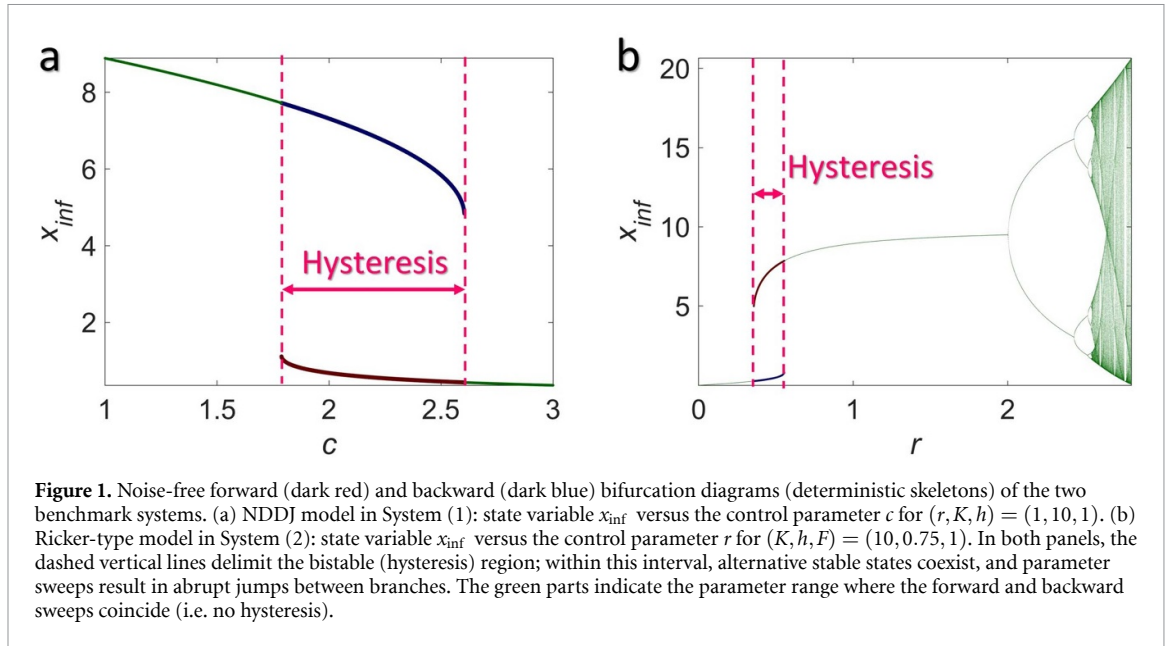
In another category, several studies have focused on evaluating early-warning methods on dynamical benchmarks, where the underlying transition mechanism is controlled, and the performance of CSD indicators can be assessed more systematically [3]. A well-known ecological benchmark is the nonparametric drift–diffusion–jump (NDDJ) model [23–25], a one-dimensional continuous-time system given by:

$$dx = \left(rx \left(1 - \frac{x}{K} \right) - \frac{cx^2}{x^2 + h^2} \right) dt + g(x_t, \theta_t) dW + dJ_t, \quad (1)$$

where x is the state variable and (r, K, c, h) are model parameters, $g(x_t, \theta_t) dW$ represents continuous stochastic forcing (Wiener noise), and dJ_t is the jump (shock) noise. The NDDJ model is attractive as a benchmark because it combines (i) a mechanistic deterministic backbone with a harvest/saturation-type nonlinearity $\frac{cx^2}{x^2+h^2}$, and (ii) two distinct stochastic components: continuous diffusion $g(x_t, \theta_t) dW$ and discrete shocks dJ_t . As a result, it can reproduce both gradual loss of resilience (captured by CSD-based trends) and abrupt, exogenous-like excursions (jumps) that can confound early-warning indicators. Figure 1(a) shows the bifurcation diagram of Model (1) in the absence of both continuous noise and shock (i.e. the deterministic skeleton), for $(r, K, h) = (1, 10, 1)$ and for $c \in [1, 3]$. As c varies, the equilibria form two stable branches separated by an intermediate unstable branch, yielding a pronounced hysteresis loop. The bistable region is bounded by two fold (saddle-node) bifurcations (marked by the dashed vertical lines), at which one of the stable equilibria disappears, and the state undergoes an abrupt transition ('jump') to the remaining branch. Consequently, forward and backward parameter sweeps follow different paths, reflecting path dependence and regime shifts. This fold-induced tipping structure makes the model particularly suitable for validating CSD measures, since indicators such as variance and lag-1 autocorrelation are expected to strengthen as the dominant eigenvalue approaches zero near the folds, while the abrupt jump provides a clear, ground-truth transition for assessing true and false warnings. Another widely used ecological benchmark for investigating CSD measures is the discrete Ricker-type model, a one-dimensional discrete-time system of the form

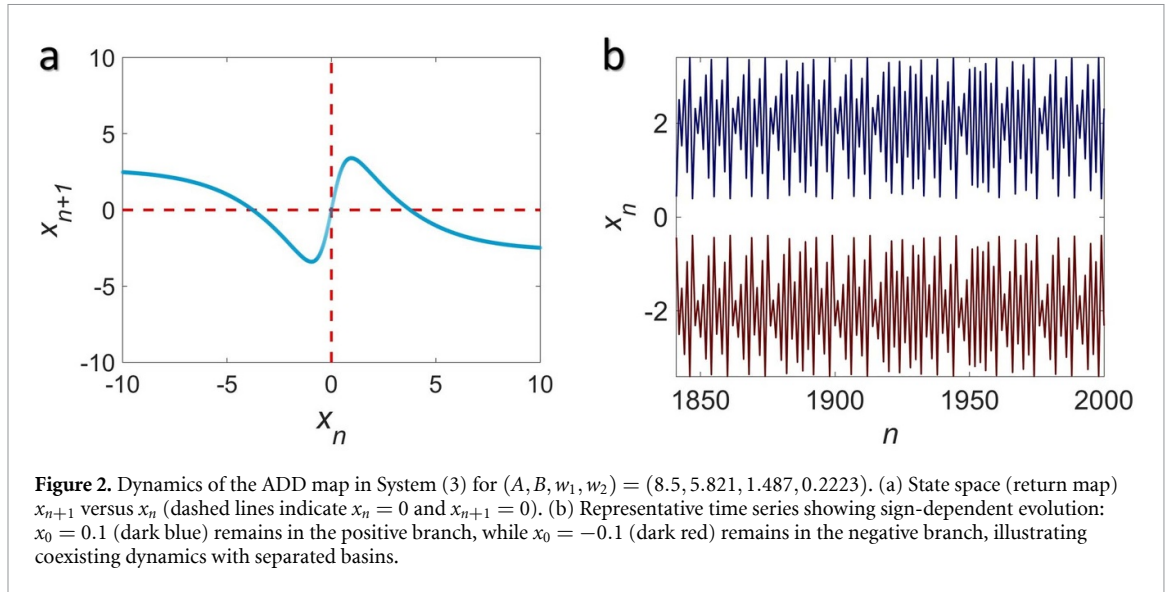
$$x_{n+1} = x_n \exp(r - bx_n + \sigma_E \varepsilon_t) - F \left(\frac{x_n^2}{x_n^2 + h^2} \right), \quad (2)$$

where x_n is the state variable representing population biomass at step n , r is the intrinsic growth rate,



and $b = \frac{r}{K}$ denotes density dependence with K as the carrying capacity. The term $\sigma_E \varepsilon_t$ models environmental stochasticity through multiplicative noise acting on growth, while the saturating loss term $F(\frac{x_n^2}{x_n^2 + h^2})$ represents harvesting/predation pressure with half-saturation parameter h . Figure 1(b) shows the bifurcation diagram of Model (2) in the deterministic setting ($\sigma_E = 0$) for $(K, h, F) = (10, 0.75, 1)$, using $r \in [0, 2.8]$ as the control parameter. For low r the system approaches a stable low-biomass equilibrium. As r increases, the diagram reveals a narrow hysteresis (bistability) window (bounded by the two dashed vertical lines) in which two alternative stable long-term states coexist; in this region, the observed outcome depends on initial conditions and sweep direction. Crossing either boundary of this window leads to an abrupt jump between the low- and high-biomass branches, indicating fold-type tipping and clear path dependence. For larger r , the high-biomass fixed point ultimately loses stability, and the diagram transitions from a single steady state to oscillatory dynamics through a period-doubling (flip) route, followed by a cascade to complex/chaotic fluctuations, as evidenced by the widening band of asymptotic values at higher r .

Different examples can be found in the literature where benchmark dynamical systems have been used to assess the capability of CSD measures [26–29]. However, benchmark systems with richer non-linear behavior are generally better suited for resembling real-world phenomena, where multiple mechanisms can shape the observed warning patterns [30]. In many applications, the underlying variability is intrinsically chaotic and intermittent [31–33], and this mechanism can generate rare but high-impact extreme events [34–36]. As illustrated above, hysteresis is an essential characteristic of many natural and engineered systems, as it implies multistability, path dependence, and abrupt regime shifts during parameter sweeps; at the same time, hysteretic systems often exhibit additional dynamical complexity beyond simple equilibrium tracking [28]. In this paper, we aim to design a dynamical system that features a hysteresis band within which distinct dynamical regimes can occur and coexist, enabling a more stringent and realistic evaluation of early-warning indicators across different transition scenarios. Notably, classic benchmark maps (e.g. NDDJ- and Ricker-type models) typically exhibit comparatively regular hysteresis dynamics, whereas our goal is to provide a benchmark in which the hysteresis band itself contains chaotic and intermittent regimes. This added dynamical richness can challenge indicators that perform well on standard models, thereby motivating the need for the proposed benchmark. The remainder of the paper is organized as follows. Section 2 presents the proposed system and the main design details, and reports its key dynamical characteristics. Section 3 evaluates four widely used CSD-based indicators—lag-1 autocorrelation, variance, skewness, and kurtosis—on the proposed benchmark and compares their performance. Section 4 concludes the paper.



2. System design

In 2015, Baghdadi *et al* [37] proposed a simple behavioral (top–down) dynamical model for the sustaining-attention problem in attention deficit disorder (ADD), based on the idea that the unwanted alternation in attention levels resembles chaotic intermittency.

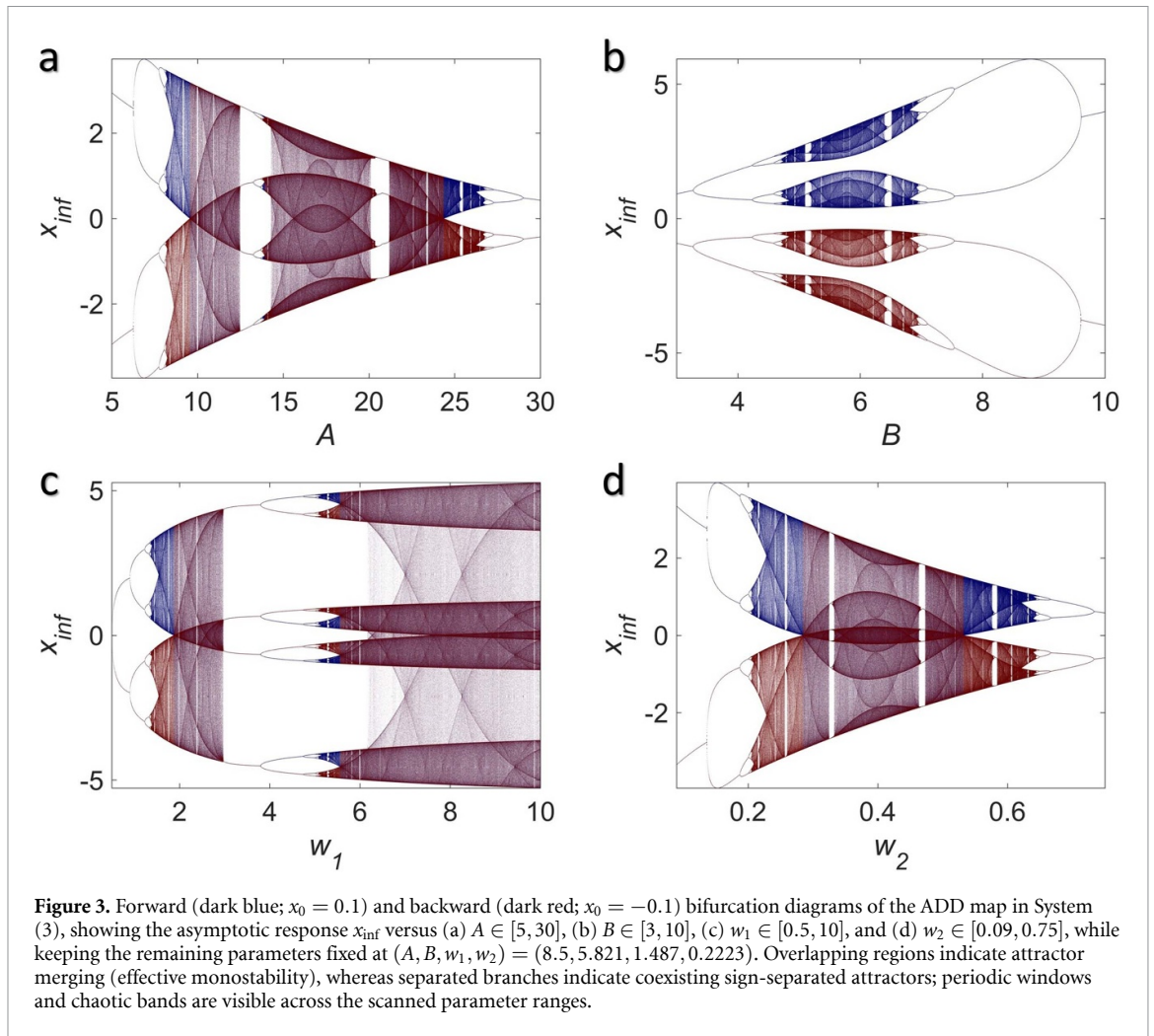
Concretely, they introduce a two-path excitatory–inhibitory neural-network-inspired map with hyperbolic-tangent activation functions whose output evolves in discrete time as a weighted difference of an excitatory and an inhibitory contribution:

$$x_{n+1} = B \tanh(w_1 x_n) - A \tanh(w_2 x_n), \quad (3)$$

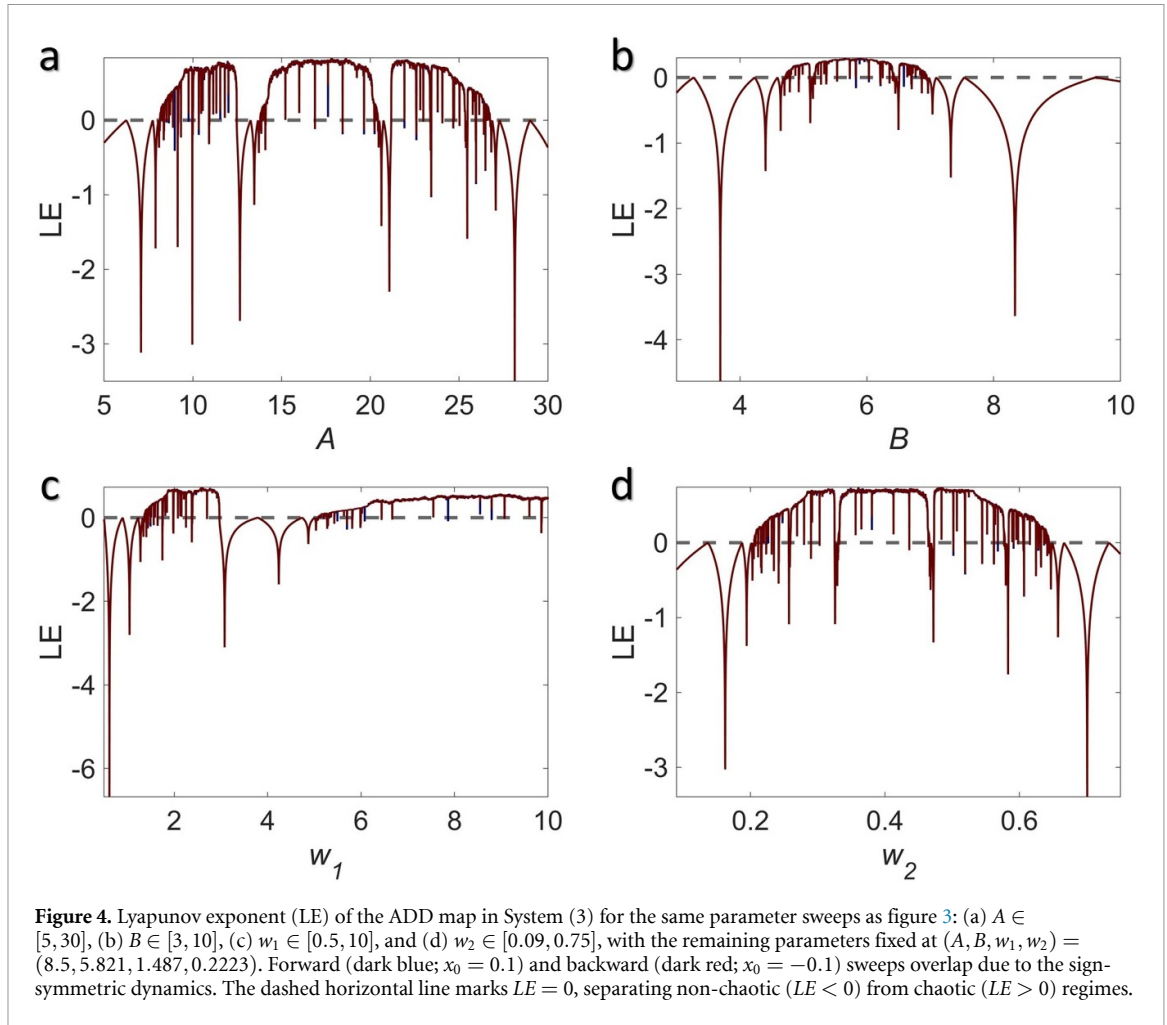
where A , B , w_1 , and w_2 represent effective synaptic gains that they interpret as being modulated by neurotransmitters. From a broader perspective, the $\tanh(\cdot)$ activation serves as a generic smooth saturating nonlinearity that enforces bounded responses and captures threshold-like regulation. Similar saturating feedback forms are widely used beyond neuroscience, for example, to model limited growth, resource saturation, or bounded forcing in ecological and climate-related models [38–40].

Assuming $A = 8.5$, $B = 5.821$, $w_1 = 1.487$, and $w_2 = 0.2223$, figure 2(a) shows the state-space (return-map) representation of the ADD model in System (3) by plotting x_{n+1} as a function of x_n . The nonlinear map has an S-shaped profile arising from the competition between the excitatory and inhibitory $\tanh(\cdot)$ terms, and it is strongly bounded since $\tanh(\cdot)$ saturates for large $|x_n|$. A key observation is that the range of the map lies within the domain (i.e., the range is a subset of the domain), implying that trajectories are confined to an invariant interval and remain bounded under iteration. Moreover, the map preserves the sign of the state in the sense that positive initial conditions generate positive dynamics, whereas negative initial conditions evolve within the negative branch, so trajectories do not cross the origin. This sign-invariant partitioning creates two dynamically disconnected basins, one on $x > 0$ and one on $x < 0$, which indicates multistability (coexisting long-term behaviors determined by the initial condition). In addition, the stretching-and-folding structure of the return map, which is visible through its pronounced nonlinear curvature, supports sensitive dependence on initial conditions, and the resulting bounded trajectories exhibit irregular, aperiodic fluctuations consistent with chaotic dynamics. For example, in figure 2(b), the dark blue signal is generated from a positive initial condition ($x_0 = 0.1$) and remains entirely in the $x > 0$ region, whereas the dark red trajectory starts from a negative initial condition ($x_0 = -0.1$) and stays confined to $x < 0$. This clear separation confirms the existence of two disjoint basins of attraction with coexisting long-term dynamics selected solely by the sign of the initial state, providing direct numerical evidence of multistability in the ADD map.

For better illustration, figure 3 presents the forward (dark blue) and backward (dark red) bifurcation diagrams of the ADD map when each parameter, i.e., A , B , w_1 , and w_2 is treated as the bifurcation parameter, while the remaining parameters are fixed at $(A, B, w_1, w_2) = (8.5, 5.821, 1.487, 0.2223)$. In panel (a), as A varies in $[5, 30]$, the system starts with two symmetric stable fixed points (one positive and one negative). As A increases, each branch undergoes a transition to more complex dynamics through a period-doubling route, evidenced by successive branch splitting and the emergence of broad



point clouds corresponding to chaotic motion. At larger A , the chaotic bands intermittently collapse into narrower branches, revealing periodic windows, and may return to lower-period dynamics through inverse period-doubling. The intervals where the forward and backward diagrams appear to merge correspond to parameter ranges where both initializations converge to the same attractor (effective monostability), so the asymptotic response becomes independent of the initial sign. On the other hand, in panel (b), no attractor-merging phenomenon is observed. Instead, as B varies in $[3, 10]$, the dynamics remain persistently sign-separated, with the positive (dark blue) and negative (dark red) attractor sets staying disjoint over the entire scanned interval. The bifurcation structure indicates repeated transitions between low-period oscillations and chaotic bands on each branch, together with intermittent periodic windows embedded within broader chaotic regimes. Importantly, although the qualitative route to complexity is similar on the two branches, the corresponding attractors do not collapse onto a common set, implying that multistability is preserved for all considered values of B , and the long-term response remains strongly dependent on the initial condition sign. Panel (c) shows that when w_1 varies in $[0.5, 10]$, attractor merging occurs in two distinct parameter intervals. In these ranges, trajectories initiated on the positive and negative sides converge to the same asymptotic set, so the forward (dark blue) and backward (dark red) diagrams largely overlap, indicating an effectively monostable response despite the sign-invariant nature observed elsewhere. Outside these intervals, the dynamics revert to coexisting sign-separated attractors, in which the two branches remain disjoint and exhibit the usual progression from low-period behavior to broader chaotic bands, with intermittent periodic windows embedded within the chaotic regimes. Panel (d), where w_2 varies in $[0.09, 0.75]$ exhibits a behavioral pattern similar to panel (a) (with A as the bifurcation parameter). Specifically, the dynamics alternate between sign-separated attractors and parameter intervals in which the attractors merge, yielding substantial overlap between the dark blue and dark red bifurcation sets and therefore an effectively monostable response. The main difference is that, within the merging band of panel (d), the embedded periodic windows are noticeably narrower (i.e., the overlap region is dominated more by chaotic dynamics and contains only



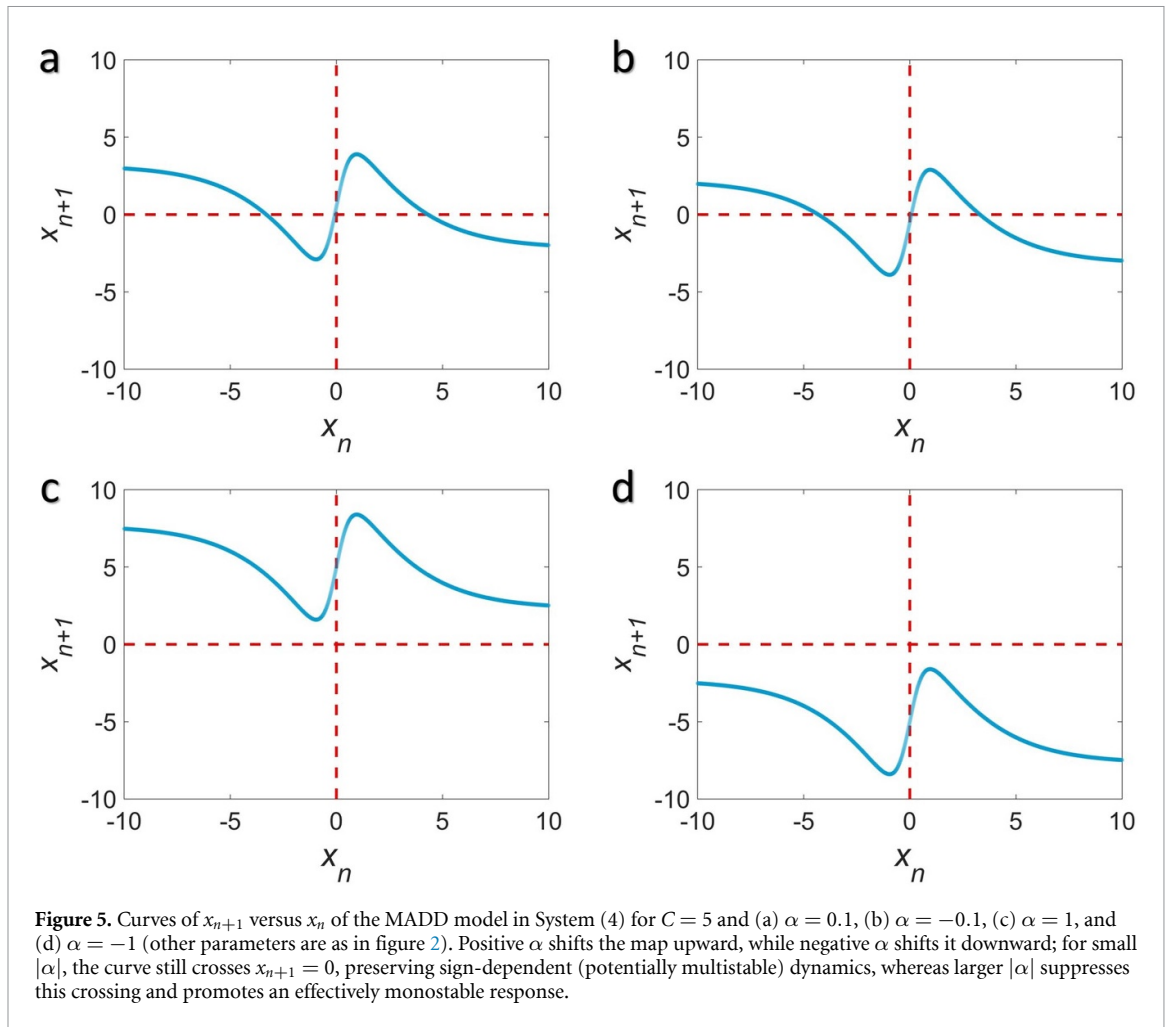
small intervals of low-periodic behavior) compared with panel (a). It should be noted that for the forward bifurcation sweeps, the initial condition is set to $x_0 = 0.1$, whereas for the backward sweeps, it is set to $x_0 = -0.1$.

Figure 4 presents the Lyapunov exponent (LE) of the ADD model for the forward ($x_0 = 0.1$) and backward ($x_0 = -0.1$) sweeps, with each panel corresponding to the same parameter scan shown in figure 3. Owing to the sign-symmetry of the map, the forward and backward trajectories evolve on symmetric invariant sets; consequently, their Lyapunov spectra are essentially identical, and the two LE curves overlap across the scanned ranges in each panel. The dashed horizontal line at $LE = 0$ separates non-chaotic and chaotic regimes: intervals with $LE > 0$ indicate chaotic dynamics, whereas $LE < 0$ corresponds to stable periodic or fixed-point behavior. The sharp negative dips are consistent with parameter windows where trajectories contract strongly (e.g. periodic windows), while the broad plateaus near or above zero match the complex bands observed in the corresponding bifurcation diagrams.

According to the dynamical properties discussed above, the ADD model is a low-dimensional, map-based system that nevertheless exhibits rich nonlinear behavior, including multistability and chaotic regimes. These features make it a suitable candidate for benchmarking EWS and evaluating the performance of CSD indicators under complex yet controllable dynamics. A closer inspection of figure 2(a) also suggests a simple mechanism for generating asymmetric multistability: adding a constant bias (DC) term shifts the map vertically and breaks sign symmetry, thereby altering the relative stability and basin structure of the coexisting attractors. Specifically, we extend the model as

$$x_{n+1} = B \tanh(w_1 x_n) - A \tanh(w_2 x_n) + C\alpha, \quad (4)$$

where α is a DC offset (bias) parameter, and C is a scaling coefficient used to control the effective shift magnitude. This symmetry-breaking term moves the return map upward or downward, enabling one branch to dominate or altering the coexistence pattern, and thereby providing a tunable setting for testing EWS performance under asymmetric basins and unequal attractor strengths.



Setting $C = 5$, figure 5 illustrates how the DC term breaks the sign symmetry of the original ADD map by vertically shifting the return curve in the modified ADD (MADD) model. Specifically, panels (a)–(d) show x_{n+1} versus x_n for $\alpha = 0.1$, $\alpha = -0.1$, $\alpha = 1$, and $\alpha = -1$, respectively. For positive α (panels (a) and (c)), the DC term shifts the map upward, whereas for negative α (panels (b) and (d)) it shifts the map downward. When $|\alpha|$ is small (e.g. $\alpha = \pm 0.1$ in panels (a) and (b)), the displacement is modest, and the curve still crosses the vertical axis (i.e. it attains $x_{n+1} > 0$ and $x_{n+1} < 0$ near $x_n = 0$). Consequently, the map continues to permit sign-dependent evolution: trajectories can remain predominantly on one side of the state space depending on the initial condition, so the system can retain multistability while exhibiting chaotic fluctuations on each side. In contrast, when $|\alpha|$ is large (e.g. $\alpha = \pm 1$ in panels (c) and (d)), the vertical shift becomes strong enough that the map is displaced almost entirely above or below the horizontal line $x_{n+1} = 0$. In this regime, the sign partitioning is effectively lost because the iterates are biased toward a single side of the state space. As a result, the dynamics become effectively monostable, typically converging to a stable fixed point or a low-period orbit, consistent with the visually smoother, less intricate dynamical structure in panels (c) and (d) compared with (a) and (b).

Accordingly, by tuning α the MADD model can be driven through qualitatively different dynamical regimes. Figure 6 shows the forward (dark blue) and backward (dark red) bifurcation diagrams (panel (a)) and the corresponding LEs (panel (b)) as functions of $\alpha \in [-1.5, 1.5]$. For large bias ($|\alpha| > 0.5$), the DC term dominates the symmetry of the original map, and the system becomes effectively monostable: trajectories are confined to a single branch and the long-term response settles to a stable fixed point or a period-2 orbit (consistent with $LE < 0$ in panel (b)). In particular, the bifurcation structure indicates a transition from a period-1 (fixed-point) regime to a period-2 regime as $|\alpha|$ increases, which is also reflected by the change in the asymptotic bands. In contrast, for moderate bias ($|\alpha| < 0.5$) the system exhibits a pronounced hysteresis-like band (marked by the dashed vertical lines), where the forward and backward sweeps follow different attracting sets. Within this interval, multiple attractors coexist, and the final state depends on the sweep direction (and initial condition), leading to abrupt

switching between the upper and lower branches at the band edges. Moreover, the bifurcation plot in panel (a) reveals complex dynamics inside this band, including broadband chaotic regions interspersed with periodic windows, which is corroborated by panel (b), where the LE becomes near-zero or positive over substantial subranges. Panel (c) further quantifies this complexity via the fractal dimension (FD) computed from the generated time series. Since the MADD dynamics are one-dimensional and yield only a single LE, an LE-based Kaplan–Yorke estimate would be degenerate and cannot provide a non-integer attractor dimension. We therefore employ a time-series box-counting-type estimator (the Liebovitch–Tóth fast algorithm [41]) to obtain an FD proxy from sampled trajectories. The FD profile closely follows the dynamical regimes identified in panels (a, b): $|\alpha| \gtrsim 0.5$, the FD collapses to values near zero, consistent with convergence to a fixed point or a low-period orbit (simple, non-fractal geometry). In contrast, within the hysteresis interval $|\alpha| \lesssim 0.5$, the FD rises markedly and fluctuates over a broad range (reaching values close to order unity), indicating a geometrically complex invariant set associated with chaotic motion, while intermittent drops correspond to periodic windows embedded in the chaotic band. Importantly, the forward (blue) and backward (red) FD curves do not coincide inside the band, mirroring the coexisting attractors and direction-dependent switching observed in panel (a). Overall, figure 6 confirms that α acts as an effective control parameter that creates a central coexistence region with direction-dependent outcomes, flanked by outer parameter ranges characterized by simpler monostable dynamics.

As a result, introducing a DC offset allows us to construct a benchmark system that combines a central coexistence (hysteresis-like) band with rich nonlinear dynamics within it. This architecture more closely resembles many real-world settings in which abrupt transitions occur under multistability and irregular variability, and therefore provides a stringent platform for assessing the robustness, false-alarm tendency, and consistency of CSD-based early-warning indicators. Moreover, because the proposed benchmark is discrete-time, it is computationally lightweight, enabling long time-series generation and large-scale parameter sweeps at low cost, which is particularly advantageous for systematic performance testing under different window sizes, sampling schemes, and noise conditions.

3. CSD indicator evaluation

In this section, we evaluate the performance of four metric-based CSD indicators on the MADD model while using α as the control parameter (see the bifurcation diagram in figure 6(a)). The considered indicators are lag-1 autocorrelation (ρ), variance (σ^2), skewness (γ_1), and kurtosis (γ_2), defined for a time series $\{x_i\}_{i=1}^N$ (after discarding transients) as

$$\rho = \frac{\sum_{i=2}^N (x_i - \mu)(x_{i-1} - \mu)}{\sum_{i=1}^N (x_i - \mu)^2}, \quad (5)$$

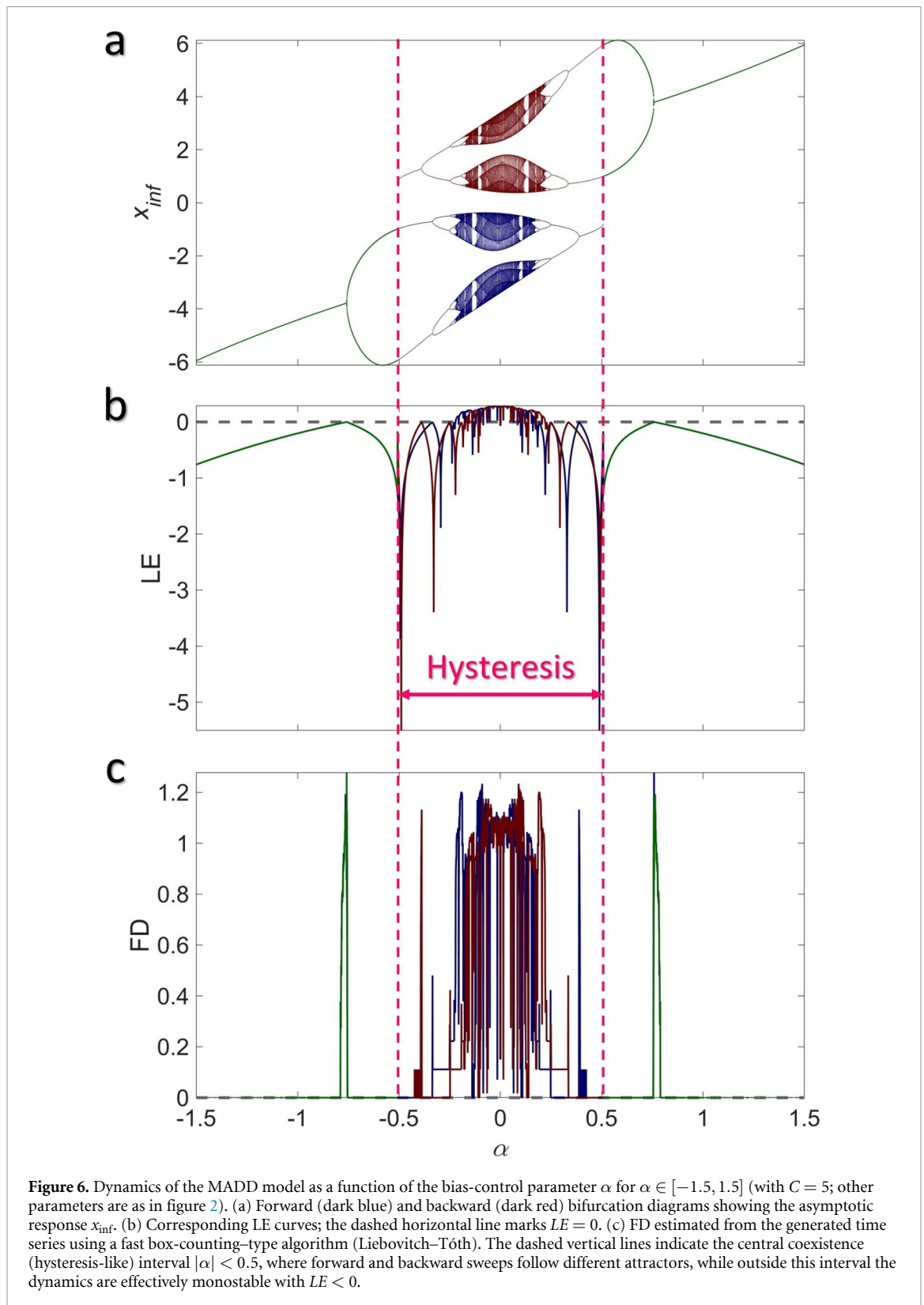
$$\sigma^2 = \frac{1}{N} \sum_{i=1}^N (x_i - \mu)^2, \quad (6)$$

$$\gamma_1 = \frac{1}{N} \frac{\sum_{i=1}^N (x_i - \mu)^4}{\sigma^4}, \quad (7)$$

$$\gamma_2 = \frac{1}{N} \frac{\sum_{i=1}^N (x_i - \mu)^3}{\sigma^3}, \quad (8)$$

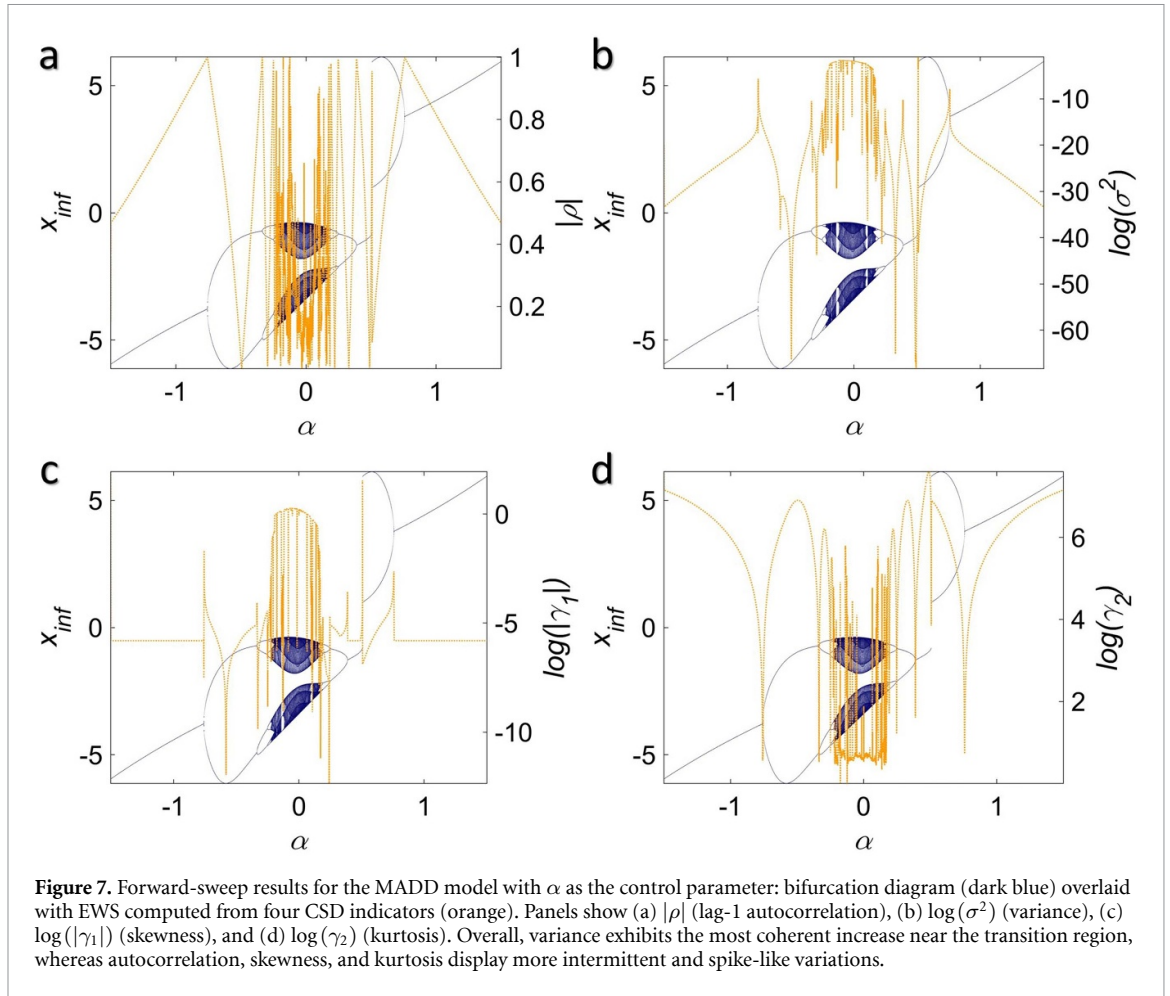
where N is the sample size, μ is the mean, and σ is the standard deviation of x_i . As EWS, we generally expect the lag-1 autocorrelation to increase and approach unity as the system loses resilience, and the variance to rise due to amplified fluctuations. In contrast, skewness and kurtosis may exhibit noticeable changes—often a reduction in their estimated values in some regimes—reflecting alterations in the distributional shape of the fluctuations as the system approaches a transition.

As emphasized by Nazarimehr *et al* [3], applying the standard (direct) CSD formulas—such as lag-1 autocorrelation, variance, skewness, and kurtosis—often yields a reliable trend only for period-one (or fixed-point) dynamics; once the system undergoes period-doubling cascades, periodic windows, or chaotic regimes, these indicators can lose their expected monotonic behavior near tipping points. To overcome this limitation, they proposed modified (improved) metric-based indicators that explicitly account for the dynamic type of the observed time series. Their approach consists of two steps: (i) estimate the dominant period m^* by computing the autocorrelation over multiple lags and selecting the



first nonzero lag at which the autocorrelation is maximized (with a finite lag cap $m_{\text{threshold}}$); when the true period exceeds this cap or the response is chaotic, the estimated period saturates at $m_{\text{threshold}}$. (ii) Decompose the signal into m^* sub-time-series (period components) by sampling every m^* th point to form vectors V_1, \dots, V_{m^*} , compute the desired indicator on each vector, and then take their average as the improved index.

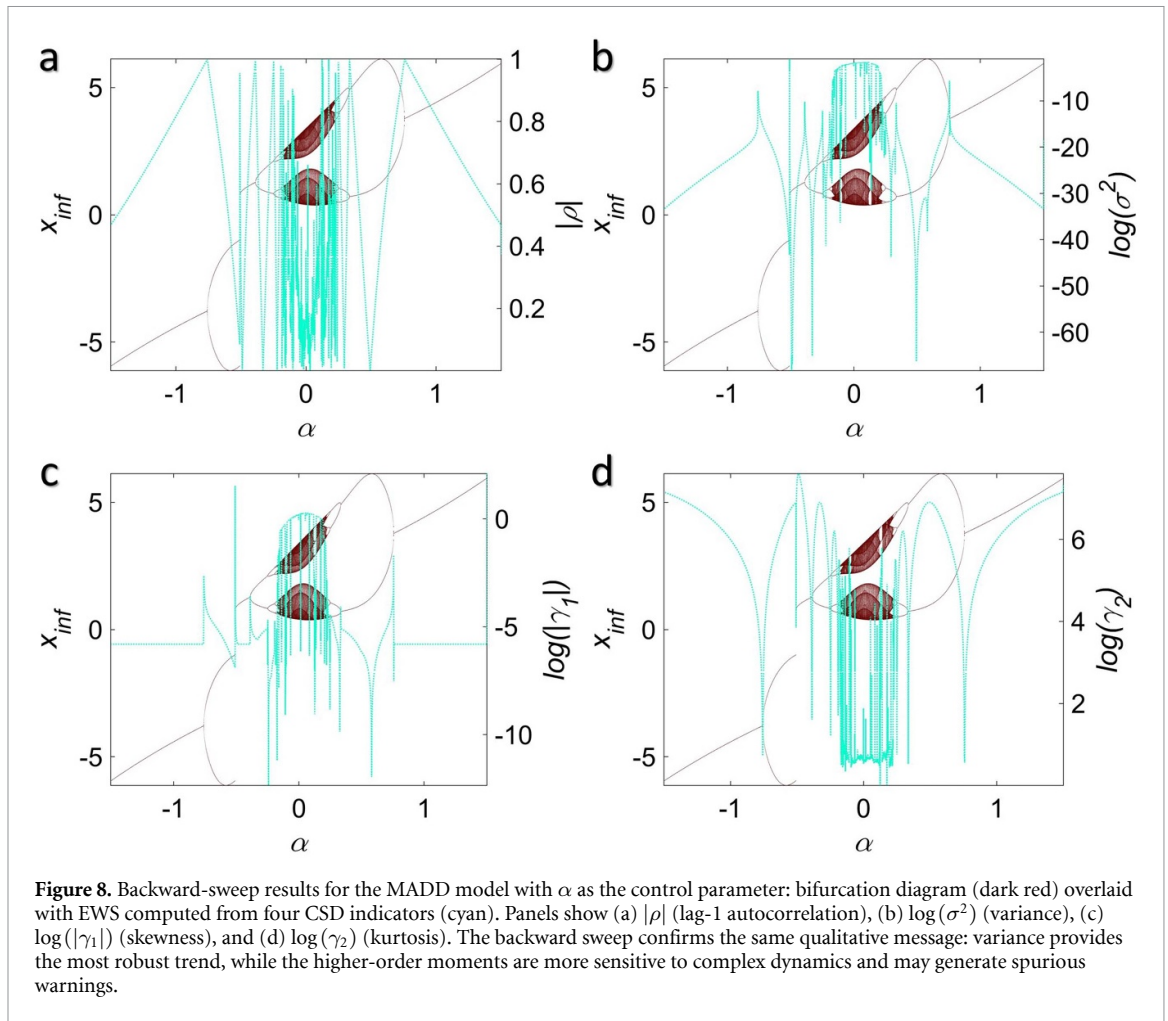
Using this modification, they reported that the improved indicators remain effective for detecting more complex transitions, including those occurring along a period-doubling route to chaos, where the



direct indicators typically fail. Thus, here, we compute the CSD indicators following the procedure in [3] and report their results for both the forward and backward sweeps. Importantly, while the period-aware approach has already been validated on standard benchmarks [3], our focus is to stress-test the same indicators under a more demanding setting—namely, a hysteresis band that contains coexisting periodic and chaotic regimes—where warning patterns can become strongly direction-dependent.

Figures 7 and 8 present the forward and backward bifurcation diagrams, respectively, along with the corresponding EWS computed from the four CSD indicators. In each panel, the bifurcation structure is shown in dark blue (forward sweep) and dark red (backward sweep), while the indicator-based EWS are overlaid using orange curves for the forward sweep and cyan curves for the backward sweep. For more precise visualization across several orders of magnitude and to avoid sign-related ambiguity, we plot the transformed measures $|\rho|$, $\log(\sigma^2)$, $\log(|\gamma_1|)$, and $\log(\gamma_2)$, corresponding to lag-1 autocorrelation, variance, skewness, and kurtosis, respectively. These overlays allow a direct comparison between changes in the dynamical regime (from the bifurcation diagram) and the expected CSD-driven trends in the statistical indicators as α approaches the transition boundaries.

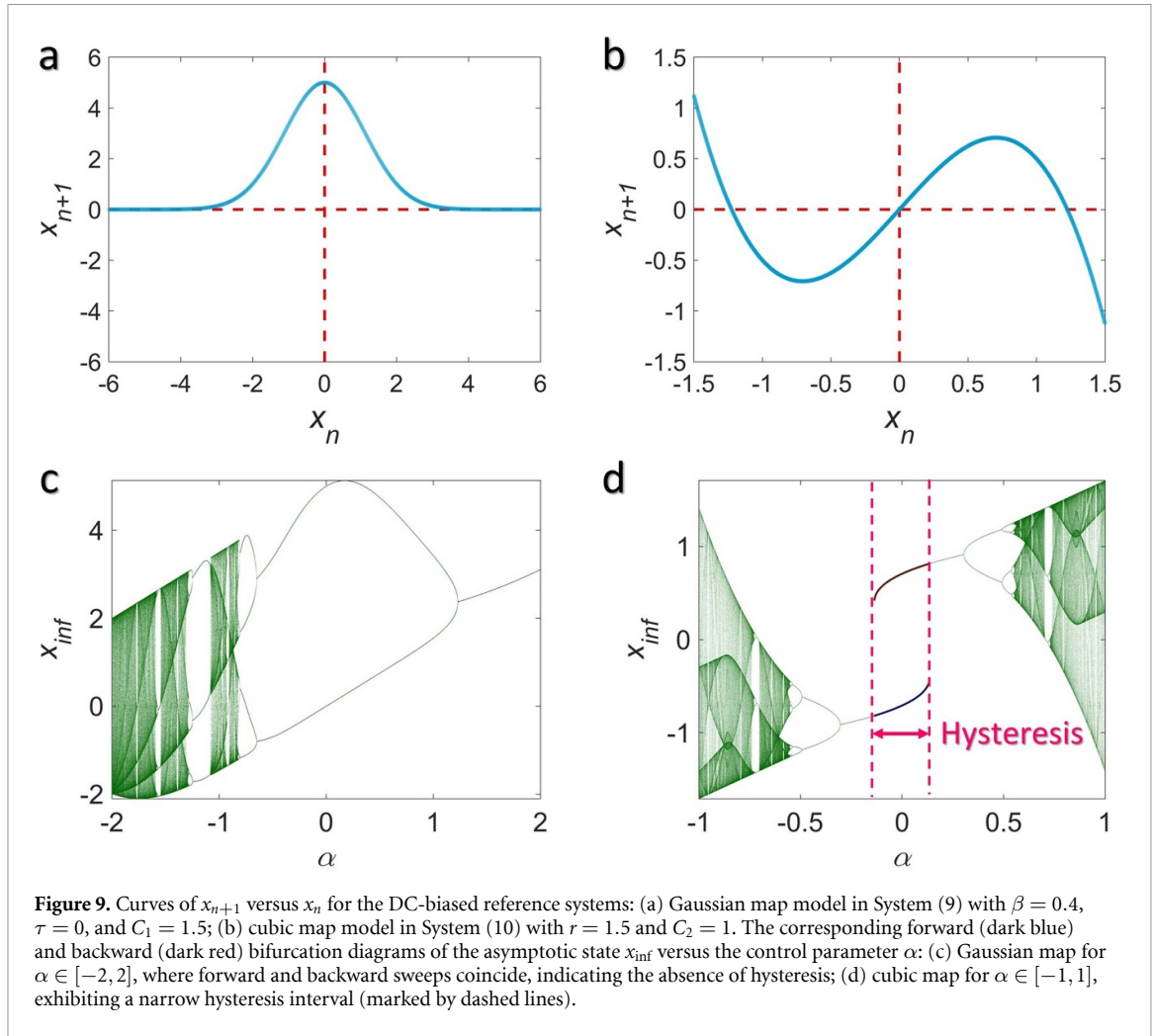
Figures 7 and 8 suggest that, among the four tested CSD indicators, variance provides the most reliable early-warning trend for the MADD benchmark. In both sweep directions, $\log(\sigma^2)$ (panels (b)) shows the clearest and most coherent change in the vicinity of the transition/coexistence region, with pronounced increases and peaks that align well with the parameter ranges where the dynamics become more complex. The lag-1 autocorrelation $|\rho|$ (panels (a)) often increases as expected, but it is noticeably more irregular and spike-dominated, indicating a higher susceptibility to spurious warnings under the intermittent/chaotic structure of the attractor. By contrast, the distribution-shape measures, $\log(|\gamma_1|)$ and $\log(\gamma_2)$ (panels (c) and (d)), exhibit strong fluctuations and abrupt jumps that do not consistently track the main transition boundaries, making skewness and kurtosis comparatively less robust indicators in this setting.



4. Conclusion

In this paper, we introduced a purpose-built dynamical benchmark for systematically validating and comparing CSD indicators under conditions closer to practical applications than those of classical clean testbeds. The proposed benchmark is constructed by starting from the ADD map model and then introducing a DC offset that breaks the original sign symmetry. This single design modification yields a controllable coexistence band (hysteresis), in which the system exhibits direction-dependent outcomes during forward/backward sweeps, while supporting rich nonlinear dynamics (periodic windows interspersed with chaotic regimes) within the coexistence region. This combination is valuable since it mimics an essential feature of many real-world transitions: abrupt shifts or jumps under multistability and path dependence, but not restricted to simple equilibrium-tracking dynamics. In addition, since the benchmark is discrete-time and low-dimensional, it supports computationally inexpensive long simulations and dense parameter scans, facilitating robust statistics and sensitivity analyses across different window lengths, sampling strategies, and experimental settings.

Using the DC term as the control parameter, we evaluated four widely used metric-based CSD indicators, i.e. lag-1 autocorrelation, variance, skewness, and kurtosis, and reported results for both forward and backward sweeps. Since complex dynamics (period-doubling, periodic windows, chaos) can invalidate the direct application of conventional CSD formulas, the indicators were computed following the period-aware procedure adopted in the literature to extend metric-based EWS to non-period-one regimes. In our benchmark, the indicator overlays in the forward/backward bifurcation diagrams show a clear qualitative ranking: variance provides the most coherent and consistently interpretable warning trend around the transition/coexistence region, whereas autocorrelation is more spike-prone (suggesting higher susceptibility to false alarms). Skewness/kurtosis are less universal in this specific hysteretic-chaotic setting due to strong sensitivity to intermittent and distribution-shape changes in complex



regimes. These observations align with the broader message that single-indicator decisions can be fragile in nonlinear and intermittently chaotic settings, and that benchmark systems with controlled yet complex structure are essential for understanding when and why EWS succeed or fail.

To show that the DC-bias mechanism by itself does not generically reproduce the MADD-type hysteresis complexity, we carried out a control comparison on two classical one-dimensional maps—a Gaussian-type map and the standard cubic map [42]—augmented by the same additive DC term used in the MADD construction:

$$x_{n+1} = Ax_n \exp(-\beta(x - \tau)) + C_1\alpha, \quad (9)$$

$$x_{n+1} = -x_n^3 + rx_n + C_2\alpha. \quad (10)$$

Here, $A = 5$, $\beta = 0.4$, $\tau = 0$, $r = 1.5$, $C_1 = 1.5$, and $C_2 = 1$. As illustrated in figures 9(a) and (b), the Gaussian map remains effectively unimodal with rapidly decaying tails, whereas the cubic map retains a two-turning-point (S-shaped) nonlinearity. This difference is reflected in the corresponding parameter sweeps (figures 9(c) and (d)): the DC-biased Gaussian map shows no hysteresis under the same sweeping protocol, with forward and backward continuations tracking the same attracting set across α . In contrast, the DC-biased cubic map can exhibit a narrow hysteresis interval. Still, the associated dynamics are comparatively simple—forward and backward continuations mainly switch between smooth, period-1 branches with limited internal structure. These control results confirm that merely adding a DC term to a generic one-dimensional map does not yield the pronounced, direction-dependent, and internally rich hysteresis band observed in the MADD model; rather, that behavior arises from the specific topological structure introduced by the ADD-to-MADD modification.

Beyond providing a new benchmark, the study highlights a practical methodological point: the difficulty of early warning detection is not determined only by whether a system has a tipping point, but

also by what happens dynamically near that tipping structure (e.g. periodic windows, crises, intermittency, and hysteresis). The proposed MADD benchmark intentionally places CSD indicators in this more demanding regime, where reliable detection must contend with direction dependence and complex attractor geometry, rather than only a smooth approach to a fold. Consequently, the benchmark can serve as a controlled test platform for (i) comparing indicator robustness, (ii) quantifying false-alarm propensity, and (iii) studying sensitivity to preprocessing and windowing choices.

While the present study focuses on proposing and characterizing a computationally efficient benchmark for stress-testing CSD indicators, several complementary analyses would further strengthen its method-oriented scope. In particular, beyond the qualitative indicator overlays reported here, a systematic quantitative performance assessment (e.g. ROC/AUC-type evaluation of detection success versus false-alarm rates) is a natural next step. In addition, the observed spike-like behavior of lag-1 autocorrelation within the coexistence band may be associated with specific dynamical events (e.g. crisis-like reorganizations or abrupt attractor changes), and a dedicated event-based diagnosis could clarify these links. Relatedly, correlating EWS strength directly with dynamical instability measures (e.g. LE-indicator correlation plots) would provide practical guidelines on parameter ranges where specific indicators become unreliable. Finally, although variance appears most coherent in the present benchmark, in chaotic regimes it may also reflect changes in attractor geometry rather than resilience loss in the classical CSD sense; disentangling these effects—together with extending the analysis to additional complexity measures such as Kolmogorov–Sinai entropy—constitutes an important direction for comprehensive future studies.

Acknowledgment

M.P. was supported by the Slovenian Research and Innovation Agency (Javna agencija za znanstvenoraziskovalno in inovacijsko dejavnost Republike Slovenije) (Grant Nos. P1-0403).

Data availability statement

No new data were created or analysed in this study.

Code availability statement

The MATLAB implementation of the period-aware indicator computation and all scripts required to reproduce the figures and results are available at <https://github.com/MahtabMehrabbeik/Complex-Hysteresis.git>.

Conflict of interest

The authors declare that they have no known competing financial interests or personal relationships that could have appeared to influence the work reported in this paper.

ORCID iDs

Mahtab Mehrabbeik  0000-0003-0336-6553

Karthikeyan Rajagopal  0000-0003-2993-7182

Veli Baysal  0000-0001-6504-1653

Matjaž Perc  0000-0002-3087-541X

References

- [1] Nazarimehr F, Jafari S, Perc M and Sprott J C 2020 Critical slowing down indicators *Europhys. Lett.* **132** 18001
- [2] Kaszás B, Feudel U and Tél T 2019 Tipping phenomena in typical dynamical systems subjected to parameter drift *Sci. Rep.* **9** 8654
- [3] Nazarimehr F, Jafari S, Golpayegani S M R H, Perc M and Sprott J C 2018 Predicting tipping points of dynamical systems during a period-doubling route to chaos *Chaos* **28** 073102
- [4] Evers K, Borsboom D, Fried E I, Hasselman F and Waldorp L 2024 Early warning signals of complex critical transitions in deterministic dynamics *Nonlinear Dyn.* **112** 19071–94

- [5] Dakos V et al 2024 Tipping point detection and early warnings in climate, ecological, and human systems *Earth Syst. Dyn.* **15** 1117–35
- [6] Dakos V, van Nes E H, D’Odorico P and Scheffer M 2012 Robustness of variance and autocorrelation as indicators of critical slowing down *Ecology* **93** 264–71
- [7] Mehrabbeik M, Ramamoorthy R, Rajagopal K, Nazarimehr F, Jafari S and Hussain I 2021 Critical slowing down indicators in synchronous period-doubling for salamander flicker vision *Eur. Phys. J. Spec. Top.* **230** 3291–8
- [8] Lenton T M, Livina V N, Dakos V, van Nes E H and Scheffer M 2012 Early warning of climate tipping points from critical slowing down: comparing methods to improve robustness *Phil. Trans. R. Soc. A* **370** 1185–204
- [9] Diks C, Hommes C and Wang J 2019 Critical slowing down as an early warning signal for financial crises? *Empir. Econ.* **57** 1201–28
- [10] Wichers M, Groot P C and Psychosystems E S (EWS Group) 2016 Critical slowing down as a personalized early warning signal for depression *Psychother. Psychosom.* **85** 114–6
- [11] Tonge N A, Miller J P, Kharasch E D, Lenze E J and Rodebaugh T L 2024 An investigation of the potential clinical utility of critical slowing down as an early warning sign for recurrence of depression *J. Behav. Ther. Exp. Psychiatry* **82** 101922
- [12] van de Leemput I A et al 2014 Critical slowing down as early warning for the onset and termination of depression *Proc. Natl Acad. Sci. USA* **111** 87–92
- [13] Smit A C, Helmich M A, Bringmann L F, Oldehinkel A J, Wichers M and Snippe E 2025 Critical slowing down in momentary affect as early warning signal of impending transitions in depression *Clin. Psychol. Sci.* **13** 760–73
- [14] Helmich M A, Schreuder M J, Bringmann L F, Riese H, Snippe E and Smit A C 2024 Slow down and be critical before using early warning signals in psychopathology *Nat. Rev. Psychol.* **3** 767–80
- [15] Tang Y, Zhu X, He C, Hu J and Fan J 2022 Critical slowing down theory provides early warning signals for sandstone failure *Front. Earth Sci.* **10** 2022
- [16] Dakos V and Bascompte J 2014 Critical slowing down as early warning for the onset of collapse in mutualistic communities *Proc. Natl Acad. Sci. USA* **111** 17546–51
- [17] Dakos V, Scheffer M, van Nes E H, Brovkin V, Petoukhov V and Held H 2008 Slowing down as an early warning signal for abrupt climate change *Proc. Natl Acad. Sci. USA* **105** 14308–12
- [18] Arumugam R, Guichard F and Lutscher F 2024 Early warning indicators capture catastrophic transitions driven by explicit rates of environmental change *Ecology* **105** e4240
- [19] Basak A, Dana S K, Bairagi N and Feudel U 2024 When do multiple pulses of environmental variation trigger tipping in an ecological system? *Chaos* **34** 093105
- [20] Maturana M I et al 2020 Critical slowing down as a biomarker for seizure susceptibility *Nat. Commun.* **11** 2172
- [21] Wilkat T, Rings T and Lehnertz K 2019 No evidence for critical slowing down prior to human epileptic seizures *Chaos* **29** 091104
- [22] Marconi M, Alfaro-Bittner K, Sarrazin L, Giudici M and Tredicce J 2024 Critical slowing down in a real physical system *Chaos Solitons Fractals* **186** 115218
- [23] Carpenter S R and Brock W A 2011 Early warnings of unknown nonlinear shifts: a nonparametric approach *Ecology* **92** 2196–201
- [24] Dakos V et al 2012 Methods for detecting early warnings of critical transitions in time series illustrated using simulated ecological data *PLoS One* **7** e41010
- [25] May R M 1977 Thresholds and breakpoints in ecosystems with a multiplicity of stable states *Nature* **269** 471–7
- [26] Marconi M, Métayer C, Acquaviva A, Boyer J, Gommel A, Quiniou T, Masoller C, Giudici M and Tredicce J 2020 Testing critical slowing down as a bifurcation indicator in a low-dissipation dynamical system *Phys. Rev. Lett.* **125** 134102
- [27] Boettner C and Boers N 2022 Critical slowing down in dynamical systems driven by nonstationary correlated noise *Phys. Rev. Phys.* **4** 013230
- [28] Tredicce J R, Lippi G L, Mandel P, Charasse B, Chevalier A and Picqué B 2004 Critical slowing down at a bifurcation *Am. J. Phys.* **72** 799–809
- [29] Meisel C, Klaus A, Kuehn C and Plenz D 2015 Critical slowing down governs the transition to neuron spiking *PLoS Comput. Biol.* **11** e1004097
- [30] Feudel U, Pisarchik A N and Showalter K 2018 Multistability and tipping: from mathematics and physics to climate and brain—minireview and preface to the focus issue *Chaos* **28** 033501
- [31] Ding X, Feng C, Wang N, Wu H and Xu Q 2025 Firing activities induced by various stimuli in a memristive ion channel-based bionic circuit *Chaos Soliton Fractals* **199** 116587
- [32] Xu Q, Wang K, Feng C, Fan W and Wang N 2024 Dynamical effects of low-frequency and high-frequency current stimuli in a memristive Morris–Lecar neuron model *Chaos Solitons Fractals* **189** 115646
- [33] Xu Q, Fang Y, Wu H, Bao H and Wang N 2024 Firing patterns and fast–slow dynamics in an n-type lam-based Fitzhugh–Nagumo circuit *Chaos Solitons Fractals* **187** 115376
- [34] Nag Chowdhury S, Ray A, Dana S K and Ghosh D 2022 Extreme events in dynamical systems and random walkers: a review *Phys. Rep.* **966** 1–52
- [35] Chowdhury S N, Majhi S, Ozer M, Ghosh D and Perc M 2019 Synchronization to extreme events in moving agents *New J. Phys.* **21** 073048
- [36] Ray A, Rakshit S, Ghosh D and Dana S K 2019 Intermittent large deviation of chaotic trajectory in Ikeda map: signature of extreme events *Chaos* **29** 043131
- [37] Baghdadi G, Jafari S, Sprott J C, Towhidkhal F and Golpayegani M R H 2015 A chaotic model of sustaining attention problem in attention deficit disorder *Commun. Nonlinear Sci. Numer.* **20** 174–85
- [38] Zaliapin I and Ghil M 2010 Another look at climate sensitivity *Nonlinear Process. Geophys.* **17** 113–22
- [39] Dortmans B, Langford W F and Willms A R 2019 An energy balance model for paleoclimate transitions *Clim. Past.* **15** 493–520
- [40] Piltz S H, Harhanen L, Porter M A and Maini P K 2018 Inferring parameters of prey switching in a 1 predator–2 prey plankton system with a linear preference tradeoff *J. Theor. Biol.* **456** 108–22
- [41] Liebovitch L S and Toth T 1989 A fast algorithm to determine fractal dimensions by box counting *Phys. Lett. A* **141** 386–90
- [42] Han X, Zhang C, Yu Y and Bi Q 2017 Boundary-crisis-induced complex bursting patterns in a forced cubic map *Int. J. Bifurc. Chaos* **27** 1750051